Journal of Stress Analysis
Vol. 7, No. 2, 2023, 27-40

Bu-Ali Sina University

ORIGINAL RESEARCH PAPER

Nonlinear Quasi-static Analysis of SMA Curved Beams

A. Cheraghback, M. Botshekanan Dehkordi*

[a]Faculty of Engineering, Shahrekord University, Shahrekord, Iran.

Article info

Article history:
Received 21 October 2022
Received in revised form
26 December 2022
Accepted 15 January 2023

Keywords:
Nonlinear quasi-static analysis
Curved SMA beam
Hernandez-Lagoudas model

Abstract

Considering many applications of Shape Memory Alloys (SMAs) in order to make structures smarter, a quasi-static analysis of curved beams made of SMA has yet to be investigated. Therefore, a quasi-static analysis of curved beams made of SMA under constant transverse force was investigated in this research. Hence, the 3D Hernandez-Lagoudas model was used to express the nonlinear properties of an SMA curved beam. For the mathematical modeling of the SMA curved beam, the Timoshenko beam theory was applied considering the nonlinear strains. Then, the governing equations were extracted using Hamilton's principle. The kinematic equations of SMAs were coupled with the governing equations of the beam, which made the analysis more complex. Differential quadrature method (DQM) in conjunction with the Newton–Raphson method was utilized to solve the nonlinear governing equations. DQM is a new numerical method based on the transformation of differential governing equations into algebra using weighting coefficients. The main objective of this paper is to obtain the martensite volume fraction, stress, and strain for all points of the beam. To validate this paper, results of static bending of a straight beam made of SMA using DQM were confirmed with other researchers' works. Numerical results showed that with the increase in the curvature radius of the curved beam, the area of the hysteresis loop was increased, indicating a decrease in the strength of the structure and, consequently, an increase in the static deflection. In addition, some new outcomes were studied for various boundary conditions. In the case of a clamped-clamped curved beam, it was concluded that at the beam's ends, the martensite volume fraction had the highest value and as it approached the center of the beam, this value decreased.

Nomenclature

σ	Stress tensor	L	Length
ε	Strain tensor	R	Radius of curvature
T	Temperature	b	Width
ξ	Martensite volume fraction	h	Thickness
ε^t	Transfer strain	k	Number of layers
α	Thermal expansion constant	u	Axial displacement
$E(\xi)$	Elastic modulus	w	Transverse displacement

*Corresponding author: M. Botshekanan Dehkordi (Associate Professor)
E-mail address: mbd_dehkordi@yahoo.com
http://dx.doi.org/10.22084/jrstan.2023.26925.1226
ISSN: 2588-2597

Λ^t	Transfer tensor	U	Potential energy
ε^{t-r}	Uniaxial transfer strain	W	External work
Φ^t	Transfer function	$N_{xx}(\xi)$	Force resultants
$f^t_{rev}(\xi)$	Forward hardening functions	$M_{xx}(\xi)$	Moment resultants
$f^t_{fwd}(\xi)$	Reverse hardening functions	$Q_{xx}(\xi)$	Shear force resultants
D	Transmission parameter	K_s	Shear correction factor
$\rho\Delta s_0$	Transmission parameter	N	Number of sample points
$\rho\Delta u_0$	Transmission parameter	C_{ij}	Weighting coefficients
C^A, C^M	Factors of the phase diagram	$[K_L]$	Linear stiffness matrix
$\{d_b\}, \{d_d\}$	Boundary and domain points	$[K_{NL}]$	Nonlinear stiffness matrix

1. Introduction

In the last few decades, SMAs, as smart and innovative materials, have found different applications in various fields of engineering due to their unique behaviors. The reversible phase-change capability of these alloys makes them able to undergo many deformations. In addition, depending on the existing temperature and stress conditions, they return to their original shape when loaded or unloaded. This capability, which is associated with a change in the mechanical, thermal, and electrical properties of the alloy, has caused SMAs to be considered as a suitable choice to be used in smart, advanced, and adaptable structures.

Here, a brief review of the articles on the analysis of SMAs in composite structures is presented. Wu et al. [1] investigated the low-velocity impact resistance of a composite plate improved by pseudo-elastic characteristics of SMA using the finite element (FE) method. They used the modified Hertz's contact law to obtain the impact force. A composite plate reinforced by SMA wires under low-velocity impact loading was investigated by Khalili et al. [2]. Hybrid composite plates reinforced by SMA wires for some important parameters under low-velocity impact loading was studied by Khalili et al. [3]. The dynamic analysis of composite plates with SMA wires was presented by Shokuhfar et al. [4]. In this paper, a hybrid composite plate during the low-velocity impact phenomena was studied in order to minimize the maximum deviation passing through. To increase the damage resistance of the composite structures under the low-velocity impact, the effects of SMA films as a reinforcement in composite plates were examined by Kim et al. [5]. Khalili et al. [6] considered the dynamic analysis of a continuous SMA hybrid composite beams subjected to impulse load, taking into account the instantaneous phase transformation at any time and also material nonlinearity effects, for every point along the beam. In their study the Brinson model is employed for modelling the SMAs. The thermal study of functionally graded SMA composites was investigated by Liu et al. [7]. Khalili et al. [8] investigated the dynamic analysis of a nonlinear continuous sandwich beam with flexible core and hybrid composite with SMA face sheets taking into account the phase transformation and also the material non-linearity effects for every point along the face sheets. The dynamic behavior of SMA hybrid composites under uniform heating after buckling of laminated beams was investigated by Asadi et al. [9]. Post-buckling behavior of Shape Memory Alloy (SMA) hybrid composite laminated beams under uniform heating was investigated.by Asadi et al. [10]. The dynamic response of nonlinear sandwich plates with flexible core and composite face-sheets embedded with SMA wires was investigated by Botshekanan Dehkordi et al. [11]. To increase the low-velocity impact resistance of composite aerosol structures with SMA properties using a numerical method in the framework of Carrera's unified formulations (CUF), a method was proposed by Hu et al. [12]. Junior et al. [13] investigated the SMA hybrid composite cylindrical stiffened panels taking into account the effects of temperature on aeroelastic stability. Thermal buckling and post-buckling of laminated composite beam reinforced with SMA wires was investigated by Bayat and Ekhteraei [14]. An analysis of post-buckling and thermal buckling of laminated composite beam reinforced with SMA wires was explored by Bayat et al. [15]. An analysis of thermal, mechanical, and thermomechanical buckling and post-buckling of symmetric laminated composite plates reinforced with SMA fibers was presented by Kabir and Tehrani [16]. Fahimi et al. [17] examined the bending response of an SMA reinforced composite beam using Brinson and Euler-Bernoulli beam models. Coherent surface theory for dynamic behavior of hybrid composite reinforced by SMA wires was investigated by Ali et al. [18]. Karimiasl et al. [19] studied post-buckling behaviors of doubly curved composite shells in hygro-thermal environments using the multiple-scale perturbation method. Enferadi et al. [20] studied wave-induced vibration control of offshore jacket platforms through SMA dampers. Nejati et al. [21] considered the thermal vibration of a double curved sandwich panel (DCSP) with embedded pre-strained SMA wire hybrid composite face sheets and soft core. Suzuki and Kagawa [22] studied the dynamic tracking control of an SMA wire actuator. Bayat and Toussi [23] studied the structural analysis of composite beams in nonlinear hybrid SMA. Shafeia and Kianoush [24] considered plasticity and damage growth in steel reinforced concrete structures with SMA wires under impact loads. Fallah et al. [25] investigated the dynamic response of microbeam containing graded shape memory microwires considering nonlinear effects. Aghababaiyan et al. [26] presented the transient nonlinear dynamic response of a micro-composite beam reinforced with carbon nanotubes (CNTs) containing SMA micro-wires considering the size effect. Fallah and Botshekanan Dehkordi [27] studied the nonlinear dynamic response of a micro composite plate embedded with micro SMA wires based on the first-order shear deformation theory considering the size effects. Kamarian and Song [28] examined the vibration analysis of composite plates with CNTs and SMA wires. Shariyat and Mirmohammadi [29] studied the time-dependent vibration response of SMA wires embedded in composite microplates considering nonlinear effects.

According to the mentioned researches, a quasi-static analysis of curved beams made of SMA has yet to be investigated. Therefore, the main contribution of this work is modelling and quasi-static analysis of SMA curved beams considering material as well as geometrical nonlinearities. In order to express the characteristics of SMAs, the 3D Hernandez-Lagoudas model is used. The Timoshenko beam theory is employed for modelling the SMA curved beam considering the nonlinear effects of strains. The governing equations are extracted using Hamilton's principle. The numerical methods of DQM and Newton–Raphson are used for solving and calculating the martensite volume fraction, stress, and strain at all points and layers of the curved beam.

2. Hernandez-Lagoudas Model

In this research, the model presented by Hernandez-Lagoudas is used for modeling the nonlinear behavior of SMAs [30]. Hernandez-Lagoudas model is an updated, complete, and exact model which can be employed for modelling the structures in a 3D form. Therefore, this model is used in this research for modeling the curved SMA beam. Lagoudas model is based on three main variables stress tensor σ, strain tensor ε, and the absolute value of temperature T and has two sub-variables of martensite volume fraction ξ and transfer strain ε^t. Total strain and stress are defined as follows [30]:

$$\varepsilon = \frac{1}{E(\xi)}(\sigma) + \alpha(T - T_0) + \varepsilon^t, \tag{1}$$

$$\sigma = E(\xi)\big[\varepsilon - \alpha(T - T_0) - \varepsilon^t\big], \tag{2}$$

Where T and α are the reference temperature and thermal expansion constant, respectively, and the elastic modulus ($E(\xi)$) is as follows [30]:

$$E(\xi) = \left[\frac{1}{E^A} + \xi\left(\frac{1}{E^M} - \frac{1}{E^A}\right)\right]^{-1} \tag{3}$$

In the above equation, the superscripts M and A denote the martensite and austenite phases, respectively. The relationship between the transfer strain rate and the martensite volume fraction rate is [30]:

$$\dot{\varepsilon}^t = \dot{\xi}\Lambda^t, \tag{4}$$

Where, Λ^t is the transfer tensor and is defined as follows:

$$\Lambda^t = \begin{cases} \Lambda^t_{fwd} = H(\sigma)\mathrm{sgn}(\sigma) & \dot{\xi} > 0 \\ \Lambda^t_{rev} = \dfrac{\varepsilon^{t-r}}{\xi^r} & \dot{\xi} < 0 \end{cases} \tag{5}$$

Where "fwd" and "rev" represent the loading and unloading phase transitions, respectively. Also, H, ε^{t-r}, and ξ^r are the uniaxial transfer strain, the transfer strain in the recovery phase, and the martensite volume fraction in the recovery phase, respectively. The transfer function (Φ^t) during the loading and unloading phase is defined according to the following equations [30]:

$$\Phi^t = \begin{cases} \Phi^t_{fwd} & 0 \le \xi \le 1 \quad \dot{\xi} \ge 0 \\ \Phi^t_{rev} & 0 \le \xi \le 1 \quad \dot{\xi} \le 0 \end{cases} \tag{6}$$

$$\begin{aligned}\Phi^t_{fwd} = {}& (1 - D)|\sigma|H(\sigma) + \frac{1}{2}\left(\frac{1}{E^M} - \frac{1}{E^A}\right)\sigma^2 \\ & + \rho\Delta s_0 T - \rho\Delta u_0 - f^t_{fwd}(\xi) - Y^t_0,\end{aligned} \tag{7}$$

$$\begin{aligned}\Phi^t_{rev} = {}& -(1 + D)\sigma\frac{\varepsilon^{t-r}}{\xi^r} - \frac{1}{2}\left(\frac{1}{E^M} - \frac{1}{E^A}\right)\sigma^2 \\ & - \rho\Delta s_0 T + \rho\Delta u_0 + f^t_{rev}(\xi) - Y^t_0,\end{aligned} \tag{8}$$

To satisfy the second law of thermodynamics, the range changes of martensite volume fraction is between zero and one and the smaller transfer function is equal to zero. In other words:

$$\Phi^t \le 0 \qquad \dot{\xi}\Phi^t = 0 \qquad 0 \le \xi \le 1 \tag{9}$$

Also, the hardening functions $f^t_{fwd}(\xi)$ and $f^t_{rev}(\xi)$ are defined as follows [30]:

$$f^t_{fwd}(\xi) = \frac{1}{2}a_1\big(1 + \xi^{n_1} - (1 - \xi)^{n_2}\big) + a_3, \tag{10}$$

$$f^t_{rev}(\xi) = \frac{1}{2}a_2\big(1 + \xi^{n_3} - (1 - \xi)^{n_4}\big) - a_3, \tag{11}$$

In the above equations, the transfer parameters D, $\rho\Delta s_0$, $\rho\Delta u_0$, Y^t_0, a_2, a_1, and a_3 are defined as follows [30]:

$$D = \left. \frac{(C^M - C^A)\big[H^{cur}(\sigma) + \sigma\partial_\sigma H^{cur}(\sigma) + \sigma(S^M_{1111} - S^A_{1111})\big]}{(C^M + C^A)\big[H^{cur}(\sigma) + \sigma\partial_\sigma H^{cur}(\sigma)\big]} \right|_{\sigma=\sigma^*}, \tag{12}$$

$$\rho\Delta s_0 = \left. \frac{-2(C^M C^A)\big[H^{cur}(\sigma) + \sigma\partial_\sigma H^{cur}(\sigma) + \sigma(S^M_{1111} - S^A_{1111})\big)}{C^M + C^A} \right|_{\sigma=\sigma^*}, \tag{13}$$

$$\rho\Delta u_0 = \frac{\rho\Delta s_0}{2}(M_s + M_f), \tag{14}$$

$$Y^t_0 = \frac{\rho\Delta s_0}{2}(M_s - M_f) - a_3, \tag{15}$$

$$a_1 = \rho\Delta s_0(M_f - M_s), \tag{16}$$

$$a_2 = \rho\Delta s_0(A_s - A_f), \tag{17}$$

$$a_3 = -\frac{a_1}{4}\left(1 + \frac{1}{n_1+1} - \frac{1}{n_2+1}\right) + \frac{a_2}{4}\left(1 + \frac{1}{n_3+1} - \frac{1}{n_4+1}\right), \tag{18}$$

Where C^A and C^M are the factors of the phase diagram and stress penetration coefficient of the austenite and martensite phases, respectively. Also, A_s, M_s, A_f, and M_f are the start of austenite phase, the end of austenite phase, the start of martensite phase, and the end of martensite phase, respectively. In addition, σ^* is the reference stress in which the mentioned parameters are obtained.

3. Governing Equations of SMA Curved Beam

The schematic of the curved beam made of SMA is shown in Fig. 1. The curved beam has the length of L, radius of curvature of R, width of b, and thickness of h. The structure is divided into k layers and the coordinate axes are considered in the middle layer of the curved beam.

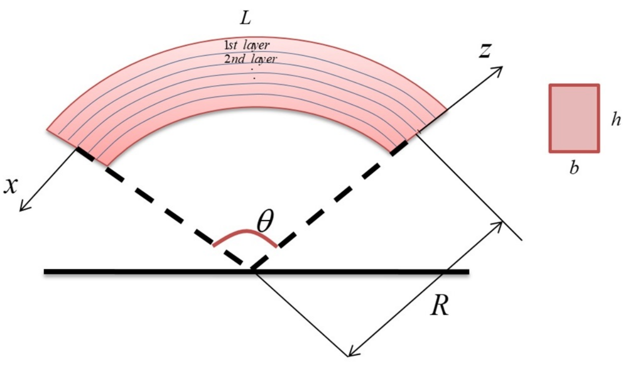

Fig. 1. Schematic of SMA curved beam made.

Using the Timoshenko beam theory, the displacement field is as follows [31]:

$$U(x,z,t) = u(x,t) + z\theta(x,t), \tag{19}$$

$$W(x,z,t) = w(x,t), \tag{20}$$

Where u and w show the displacement of the middle plane along the length and thickness directions, respectively. It should be noted that the middle plane $z = 0$ is for the case where the z coordinates are in line with the thickness of the beam. Using the mentioned displacement field, the nonlinear strain-displacement relationships in term of the martensite volume fraction become as follows:

$$\varepsilon^k_{xx}(\xi) = \frac{\partial}{\partial x}u(\xi) + z\frac{\partial}{\partial x}\theta(\xi) + \frac{1}{2}\left(\frac{\partial}{\partial x}w(\xi)\right)^2 - \frac{w(\xi)}{R}, \tag{21}$$

$$\varepsilon^k_{xz}(\xi) = \frac{\partial}{\partial x}w(\xi) + \theta(xi) + \frac{u(\xi)}{R}\cdot \tag{22}$$

According to Hooke's law, the relationship between stress-strain for each layer of the curved beam in term of the martensite volume fraction is written as follows:

$$\sigma^k_{xx}(\xi) = E^k(\xi)\big[\varepsilon^k_{xx}(\xi) - \alpha^k(\xi)(T - T_0) - \varepsilon^{tk}_{xx}(\xi)\big], \tag{23}$$

$$\sigma^k_{xz}(\xi) = \frac{E^k(\xi)}{2(1 + \upsilon^k(xi))}\big(\varepsilon^k_{xz}(\xi) - \varepsilon^{tk}_{xz}(\xi)\big), \tag{24}$$

Where the elastic modulus and Poisson's ratio of each layer of the curved beam are calculated as follows:

$$E^k(\xi) = E_A - \xi(E_M - E_A), \tag{25}$$

$$\upsilon^k(\xi) = \upsilon_A - \xi(\upsilon_M - \upsilon_A). \tag{26}$$

The longitudinal and shear strain of transfer are as follows:

$$\varepsilon^{tk}_{xx} = H^{\max}\frac{\sigma^k_{xx}(\xi)}{\sqrt{\sigma^k_{xx}(\xi)^2 + 3\sigma^k_{xz}(\xi)^2}}\xi, \tag{27}$$

$$\varepsilon^{tk}_{xz} = H^{\max}\frac{\sigma^k_{xz}(\xi)}{\sqrt{\sigma^k_{xx}(\xi)^2 + 3\sigma^k_{xz}(\xi)^2}}\xi. \tag{28}$$

The potential energy of the curved beam made of SMA is as follows:

$$\delta U=\int_0^L\int_A(\sigma_{xx}\delta\varepsilon_{xx}+\sigma_{xz}\delta\varepsilon_{xz})dAdx$$

$$=\int_0^L\int_A\sigma_{xx}\left(\frac{\partial\delta u(\xi)}{\partial x}+z\frac{\partial\delta\theta(\xi)}{\partial x}+\frac{\partial w(\xi)}{\partial x}\frac{\partial\delta w(\xi)}{\partial x}-\frac{\partial w(\xi)}{R}\right)$$

$$+\sigma_{xz}\left(\frac{\partial\delta w(\xi)}{\partial x}+\delta theta(xi)+\frac{\delta u(\xi)}{R}\right)dAdx. \quad (29)$$

The external force work of the curved beam made of SMA under constant transverse load is as follows:

$$\delta W=\int_0^L\int_A q_)\delta w dx. \quad (30)$$

Finally, using Hamilton's principle $\left(\int_0^0(\delta U-\delta W)dt=0\right)$, the governing equations of the structure are extracted as follows:

$$\delta u:\ \frac{\partial N_{xx}(\xi)}{\partial x}-\frac{Q_{xz}(\xi)}{R}=0, \quad (31)$$

$$\delta w:\ \frac{\partial Q_{xz}(\xi)}{\partial x}-\frac{N_{xx}(\xi)}{R}+\frac{\partial}{\partial x}\left(N_{xx}(\xi)\frac{\partial w(\xi)}{\partial x}\right)=q_0, \quad (32)$$

$$\delta\theta:\ \frac{\partial M_{xx}(\xi)}{\partial x}-Q_{xz}(\xi)=0, \quad (33)$$

Where the force and moment resultants are defined as follows:

$$N_{xx}(\xi)=\sum_{k=1}^{Nk}\int_{z_k}^{z_{k+1}}bE^k(\xi)(\varepsilon_{xx}^k-\varepsilon_{xx}^{t^k}(\xi))dz$$

$$=\left(A_{11}(\xi)\frac{\partial u(\xi)}{\partial x}+B_{11}(\xi)\frac{\partial\theta(\xi)}{\partial x}+\frac{A_{11}(\xi)}{2}\left(\frac{\partial w(\xi)}{\partial x}\right)^2\right.$$

$$\left.-A_{11}(\xi)\frac{\delta w(\xi)}{R}\right)-N_\xi^{SMA}, \quad (34)$$

$$M_{xx}(\xi)=\sum_{k=1}^{Nk}\int_{z_k}^{z_{k+1}}bE^k(\xi)(\varepsilon_{xx}^k-\varepsilon_{xx}^{t^k}(\xi))zdz$$

$$=\sum_{k=1}^{Nk}\int_{z_k}^{z_{k+1}}zdz=B_{11}(\xi)\frac{\partial u(\xi)}{\partial x}+D_{11}(\xi)\frac{\partial\theta(\xi)}{\partial x}$$

$$+\frac{B_{11}(\xi)}{2}\left(\frac{\partial w(\xi)}{\partial x}\right)^2-B_{11}(\xi)\frac{\delta w(\xi)}{R}-M_\xi^{SMA}, \quad (35)$$

$$Q_{xz}(\xi)=\sum_{k=1}^{Nk}\int_{z_k}^{z_{k+1}}\frac{bE^k(\xi)}{2(1+\upsilon^k(xi))}\left(\varepsilon_{xz}^k(\xi)-\varepsilon_{xz}^{tk}(\xi)\right)$$

$$=A_{11}(\xi)\frac{\partial w(\xi)}{\partial x}+A_{55}(\xi)\frac{u(\xi)}{R}-Q_\xi^{SMA}, \quad (36)$$

In the above, Q_ξ^{SMA}, M_ξ^{SMA}, N_ξ^{SMA} relationships, force, moment, and shear force are related to SMA, which are defined as follows:

$$N_\xi^{SMA}=\sum_{k=1}^{kN}\int_{z_k}^{z_{k+1}}bE^k(\xi)\varepsilon_{xx}^{t^k}(\xi)dz, \quad (37)$$

$$M_\xi^{SMA}=\sum_{k=1}^{kN}\int_{z_k}^{z_{k+1}}bE^k(\xi)\varepsilon_{xx}^{t^k}(\xi)zdz, \quad (38)$$

$$-Q_\xi^{SMA}=\sum_{k=1}^{Nk}\int_{z_k}^{z_{k+1}}b\frac{E^k(\xi)}{2(1+\upsilon^k(xi))}\varepsilon_{xz}^k(\xi). \quad (39)$$

Also, the constants $A_{11}(xi)$, $B_{11}(xi)$, $D_{11}(xi)$, $A_{55}(xi)$ are as follows:

$$A_{11}(\xi)=\sum_{k=1}^{kN}\int_{z_k}^{z_{k+1}}bE^k(\xi)dz, \quad (40)$$

$$B_{11}(\xi)=\sum_{k=1}^{kN}\int_{z_k}^{z_{k+1}}bE^k(\xi)zdz, \quad (41)$$

$$D_{11}(\xi)=\sum_{k=1}^{kN}\int_{z_k}^{z_{k+1}}bE^k(\xi)z^2dz, \quad (42)$$

$$A_{55}(\xi)=\sum_{k=1}^{kN}\int_{z_k}^{z_{k+1}}\frac{bE^k(\xi)}{2(1+\upsilon^k(xi))}dz, \quad (43)$$

Where K_s is the shear correction factor.

4. Numerical Solution

The differential quadrature method is one of the numerical methods in which the governing final coupled equations are transformed into algebraic relations using the weight coefficients. Hence, the function derivative can be written as a linear sum of weight coefficients at each point. The main relationship of DQM for a one-dimensional problem is expressed as follows [32]:

$$\frac{df(x)}{dx}=\sum_{j=1}^{n}C_{ij}f_j(x), \quad (44)$$

Where $f(x)$ is a function, N is the number of sample points, and C_{ij} is the weighting coefficients to obtain the function derivative at each point. Gridding of points along the length of the beam according to the Chebyshev transition distance is obtained as follows:

$$x_i=\frac{L}{2}\left[1-\cos\left(\frac{i-1}{N_s-1}\right)\pi\right]\qquad i=1,\cdots,N \quad (45)$$

Also, the weight coefficients for the one-dimensional problem are obtained as follows:

$$C_{ij}^{(1)} = \begin{cases} \dfrac{M(x_i)}{(x_i - x_j)M(x_j)} & \text{for } i \neq j,\ i,j = 1,2,...,N_x \\ -\sum\limits_{\substack{j=1 \\ i\neq j}}^{x} C_{ij}^{(1)} & \text{for } i \neq j,\ i,j = 1,2,...,N_x \end{cases} \tag{46}$$

Where in the above relations:

$$M(x_i) = \prod_{\substack{j=1 \\ i\neq j}}^{N_x} (x_i - x_j) \tag{47}$$

Also, for the higher order derivative, we have:

$$C_{ij}^{(n)} = n\left(C_{ii}^{(n-1)}C_{ij}^{(1)} - \frac{C_{ij}^{(n-1)}}{(x_i - x_j)}\right) \quad i \neq j \tag{48}$$

In this method, the derivatives are replaced by their respective weight coefficient matrices. Using the above equations, the governing equations in the form of DQM are as follows:

$$\begin{aligned} & A_{11}\sum_{j=1}^{N} C_{ij}^{(2)}u_j(x,t) - \frac{A_{11}}{R}\sum_{j=1}^{N} C_{ij}w_j(x,t) + B_{11}\sum_{j=1}^{N} C_{ij}^{(2)}\theta_j(x,t) \\ & + A_{11}\sum_{j=1}^{N} C_{ij}w_j(x,t)\sum_{j=1}^{N} C_{ij}^{(2)}w_j(x,t) - \frac{A_{55}}{R}\sum_{j=1}^{N} C_{ij}w_j(x,t) - \frac{A_{55}}{R^2}u_j(x,t) \\ & - \frac{A_{55}}{R}\theta_i(x,t) + \frac{Q_\xi^{SMA}}{R} = 0, \end{aligned} \tag{49}$$

$$\begin{aligned} & A_{55}\sum_{j=1}^{N} C_{ij}w_j(x,t) + \frac{A_{55}}{R}u_i(x,t) + A_{55}\theta_i(x,t) - Q_\xi^{SMA} \\ & - B_{11}\sum_{j=1}^{N} C_{ij}^{(2)}u_j(x,t) + \frac{B_{11}}{R}\sum_{j=1}^{N} C_{ij}w_j(x,t) \\ & - D_{11}\sum_{j=1}^{N} C_{ij}^{(2)}\theta_j(x,t) - B_{11}\sum_{j=1}^{N} C_{ij}w_j(x,t)\sum_{j=1}^{N} C_{ij}^{(2)}w_j(x,t) = 0, \end{aligned} \tag{50}$$

$$\begin{aligned} & A_{55}\sum_{j=1}^{N} C_{ij}w_j(x,t) + \frac{A_{55}}{R}\sum_{j=1}^{N} C_{ij}u_j(x,t) + A_{55}\sum_{j=1}^{N} C_{ij}\theta_j(x,t) \\ & - \frac{A_{11}}{R}\sum_{j=1}^{N} C_{ij}u_j(x,t) + \frac{A_{11}}{R^2}w_i(x,t) - \frac{B_{11}}{R}\sum_{j=1}^{N} C_{ij}\theta_j(x,t) \\ & - \frac{A_{11}}{2R}\sum_{j=1}^{N} C_{ij}w_j(x,t)\sum_{j=1}^{N} C_{ij}w_j(x,t) + \frac{N_\xi^{SMA}}{R} \\ & \left[\begin{array}{l} A_{11}\sum_{j=1}^{N} C_{ij}^{(2)}u_j(x,t) - \frac{A_{11}}{R}\sum_{j=1}^{N} C_{ij}w_j(x,t) + B_{11}\sum_{j=1}^{N} C_{ij}^{(2)}\theta_j(x,t) \\ +A_{11}\sum_{j=1}^{N} C_{ij}w_j(x,t)\sum_{j=1}^{N} C_{ij}^{(2)}w_j(x,t) \end{array}\right]\sum_{j=1}^{N} C_{ij}w_j(x,t) + \\ & \left[\begin{array}{l} A_{11}\sum_{j=1}^{N} C_{ij}u_j(x,t) - \frac{A_{11}}{R}w_j(x,t) + B_{11}\sum_{j=1}^{N} C_{ij}^{(2)}\theta_j(x,t) \\ +\frac{A_{11}}{2}\sum_{j=1}^{N} C_{ij}w_j(x,t)\sum_{j=1}^{N} C_{ij}w_j(x,t) - N_\xi^{SMA} \end{array}\right]\sum_{j=1}^{N} C_{ij}^{(2)}w_j(x,t) = 0. \end{aligned} \tag{51}$$

Boundary condition equations are coupled with the governing final equations. As a result, the points related to the boundary condition and the domain can be separated as boundary and domain points. Therefore, the boundary and governing final equations may be expressed in the form of a matrix as follows:

$$\left(\left[\underbrace{K_L + K_{NL}}_{K}\right]\right)\left\{\begin{array}{c}\{d_b\}\\ \{d_d\}\end{array}\right\} = \left\{\begin{array}{c}\{0\}\\ \{F\}\end{array}\right\}, \tag{52}$$

Where F represents the transverse force on the curved beam. Also, $\{d_b\}$ and $\{d_d\}$ are the boundary and domain vectors corresponding to the boundary points, respectively. Also, $[K_L]$ and $[K_{NL}]$ are the linear part of the stiffness matrix and the nonlinear part of the stiffness matrix, respectively, which are as follows:

- ***Linear matrix:***

$$K_{L11} = A_{11}C^2 - \frac{A_{55}I}{R^2}, \tag{53a}$$

$$K_{L12} = B_{11}C^2 - \frac{A_{55}I}{R}, \tag{53b}$$

$$K_{L13} = \frac{-A_{11}C - A_{55}C}{R}, \tag{53c}$$

$$K_{L21} = \frac{A_{55}I}{R} - B_{11}C^2, \tag{53d}$$

$$K_{L22} = A_{55}I - D_{11}C^2, \tag{53e}$$

$$K_{L23} = A_{55}C + \frac{B_{11}C}{R}, \tag{53f}$$

$$K_{L31} = \frac{A_{55}C}{R} - \frac{A_{11}C}{R}, \tag{53g}$$

$$K_{L32} = A_{55}C - \frac{B_{11}C}{R}, \tag{53h}$$

$$K_{L33} = A_{55}C^2 + \frac{A_{11}I}{R^2} - N_{\xi}^{SMA}C^2, \tag{53i}$$

- ***Nonlinear matrix:***

$$K_{NL11} = Z, \tag{54a}$$

$$K_{NL12} = Z, \tag{54b}$$

$$K_{NL13} = A_{11}(Cw)C^2, \tag{54c}$$

$$K_{NL21} = Z, \tag{54d}$$

$$K_{NL22} = Z, \tag{54e}$$

$$K_{NL23} = -B_{11}(Cw)C^2, \tag{54f}$$

$$K_{NL31} = A_{11}(C^2w)C + A_{11}(Cw)C^2, \tag{54g}$$

$$K_{NL32} = B_{11}(C^2w)C + B_{11}(Cw)C^2, \tag{54h}$$

$$K_{NL33} = -\frac{A_{11}}{2R}(Cw)C - \frac{A_{11}}{R}(Cw)C + A_{11}(Cw)(C^2w)C$$
$$-\frac{A_{11}}{R}(Iw)C^2 + \frac{A_{11}}{R}(Cw)(Cw)C^2. \tag{54i}$$

Where C is the weight coefficients and Z is the zero matrix. The above equation is a nonlinear equation and the process of solving it for the nonlinear state is as follows (Newton–Raphson method):

1. The nonlinear terms in the stiffness matrix are ignored and the displacement vector $\{d\}$ is calculated in the linear state.
2. The obtained displacement vector is placed in the nonlinear terms of the stiffness matrix and the displacement vector corresponding to the nonlinear state is calculated again.
3. Then, the displacement vector is compared with the displacement vector of the previous step and this process continues until the following convergence ratio is satisfied:

$$\frac{d_{i+1} - d_i}{d_{i'}} < 0.01 \tag{55}$$

5. Convex Cutting-plane Return Mapping Algorithm

As mentioned above, first, the nonlinear displacement of the curved beam made of SMA is calculated using DQM. Then, using the convex cutting-plane return mapping algorithm, the martensite volume fraction, stress, and strain are calculated at any point of each layer of the curved beam. This algorithm solves the thermoelastic transfer problem which is defined by the relationship of total strain, flow law, and transfer function by dividing the problem into two consecutive processes. In the first process, according to a thermoelastic prediction, it is assumed that the transfer strain is zero. If this prediction leads to the violation of the transfer criterion $\psi^t \leq 0$, according to the second process, a series of transfer correction relations will be used to satisfy the mentioned transfer criterion. This algorithm includes the following steps [33]:

I At the beginning of loading, the default values of martensite volume fraction, transfer tensor, and transfer strain are assumed to be zero.

II The values of Young's modulus $E(\xi)$, constants $A_{11}(xi)$, $B_{11}(xi)$, $D_{11}(xi)$, $A_{55}(xi)$,internal forces, and SMA moments (Q_{ξ}^{SMA}, M_{ξ}^{SMA}, N_{ξ}^{SMA}) are calculated.

III Longitudinal and shear strains are calculated with the help of non-linear displacement obtained by the DQM.

IV Softness tensor $S(\xi)$ and then the values of axial and shear stress $(\sigma_{xx}(\xi), \sigma_{xz}(\xi))$ are calculated and finally the equivalent stress is calculated using the von Mises criterion.

V The transfer function has two states. If the transfer function is smaller than or equal to zero $(\phi(\xi) \leq 0)$, the martensite volume fraction , stress, strain, and calculated transfer strain are final, provided that the difference of the martensite volume fraction calculated with the value of the previous step is insignificant.

VI If the transfer function is not smaller than or equal to zero, the correction values of martensite volume fraction should be assumed. In other words:]

- Calculate $\Delta\xi_{n+1}^{(k)} = \dfrac{-\phi_{n+1}^{t(k)}}{A^t}$ which $A_\xi^\partial \phi_{n+1}^{t(k)} : \mathbf{S}_{n+1}^{-1(k)}(\Delta\mathbf{S}\boldsymbol{\sigma}_{n+1}^{(k)} + \boldsymbol{\Lambda}_{n+1}^{t(k)})$
- Calculate $\xi_{n+1}^{(k+1)} = \xi_{n+1}^{(k)} + \Delta\xi_{n+1}^{(k)}$ and $\boldsymbol{\varepsilon}_{n+1}^{(k+1)} = \boldsymbol{\varepsilon}_{n+1}^{(k)} + \Delta\xi_{n+1}^{(k)} + \boldsymbol{\Lambda}_{n+1}^{t(k)}$
- If $0 \leq \xi_{n+1}^{(k+1)} \leq 1$ Let the steps be continued, otherwise, $\xi_{n+1}^{(k+1)}$ set at the boundary of the mentioned range and $\delta\xi_{n+1}^{(k)}$, $\xi_{n+1}^{(k+1)}$ and $\boldsymbol{\varepsilon}_{n+1}^{t(k+1)}$ is recalculated.

The convex-cutting plane return mapping algorithm is shown in Fig. 2.

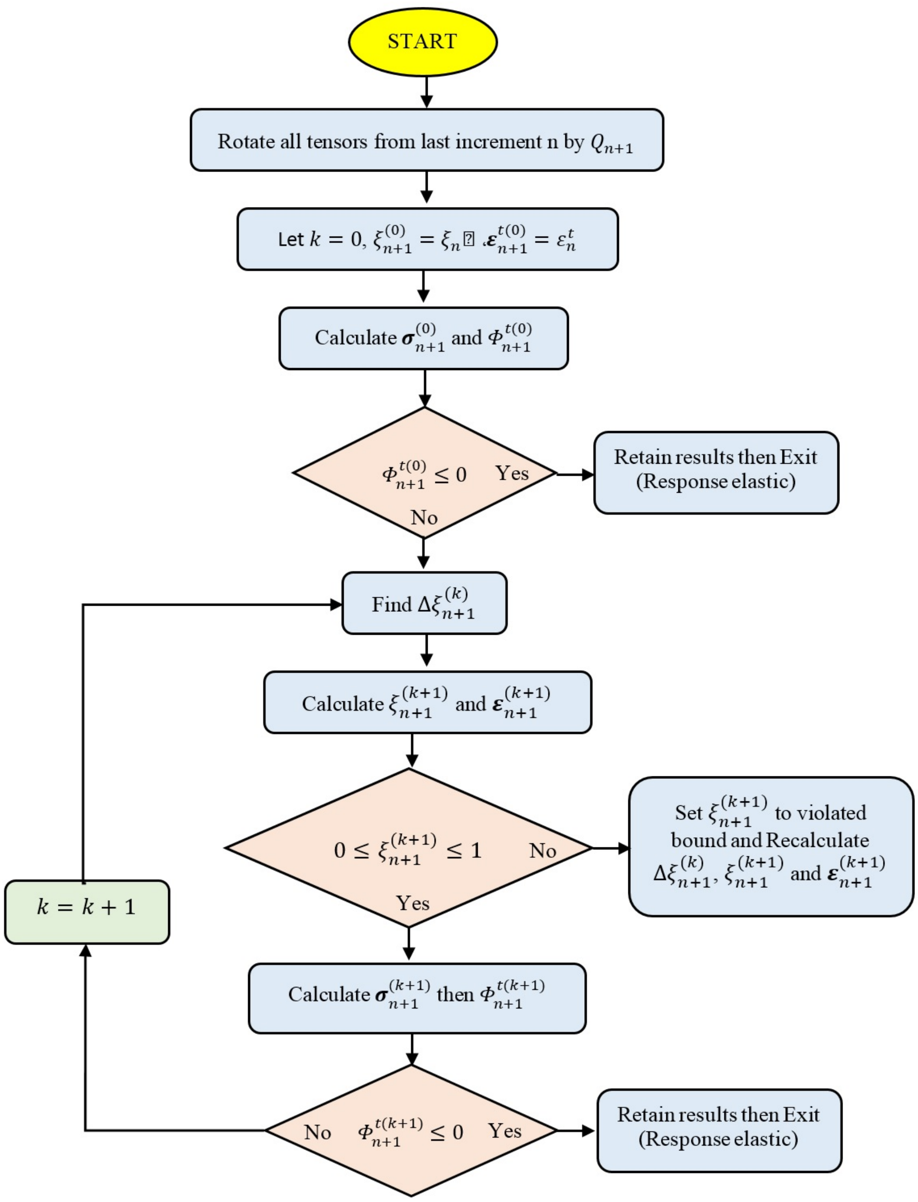

Fig. 2. Convex cutting-plane return mapping algorithm.

VII This process is repeated for each stage of loading and unloading and for each point at each layer of the curved beam until the martensite volume fraction, stress, and strain are finally derived.

6. Numerical and Results Discussion

In this part, an SMA curved beam made from nickel-titanium (NiTi) with the properties presented in Table 1 is used to express the results [34]. The results are presented for different loading and unloading conditions at constant temperature T=T0=300 K. To express the results, a clamped-clamped curved beam with a length of 5 m, curvature radius of 1.2 m, and thickness of 0.3 m is assumed. The results of this section are presented for the middle point of the clamped beam and the upper layer. This part includes three parts: convergence of the numerical solution, validation of the outcomes, and investigation of the quasi-static behavior of the SMA curved beam.

Table 1
Properties of nickel-titanium SMA [34].

Properties	Unit
H	0.03
A_s	217K
A_f	290K
M_s	264K
M_f	160K
$\upsilon^A = \upsilon^M$	0.3
E_A	32.5GPa
E_M	23GPa
$\rho\Delta S_0$	-0.11e6 J/m3K
ΔC	1e-4

6.1. Convergence of Numerical Method

Table 2 shows the convergence and accuracy of the numerical solution. In this table, the transverse deflection of the middle point of the curved beam is shown in the dimensionless form (w/h) for the end of the loading phase. The results show that in $N = 21$, the results are converged and that the increase of grid points has no effect on the rise of the structure's deflection.

Table 2
Convergence of DQM for static deflection.

N	w/h
15	0.0057
17	0.0127
19	0.0170
21	0.0174
23	0.0174

Fig. 3 shows the static bending diagram of the curved beam for the middle point of the beam and the top layer along the length for the clamped-clamped boundary condition at the beginning of the loading stage. It can be seen that with the increase in the number of layers, the deflection decreases. Also, the deflection of the structure at the end of the loading stage is more than that at the beginning of loading, which seems reasonable. In addition, with the increase in the number of layers, the rate of changes in the deflection decreases.

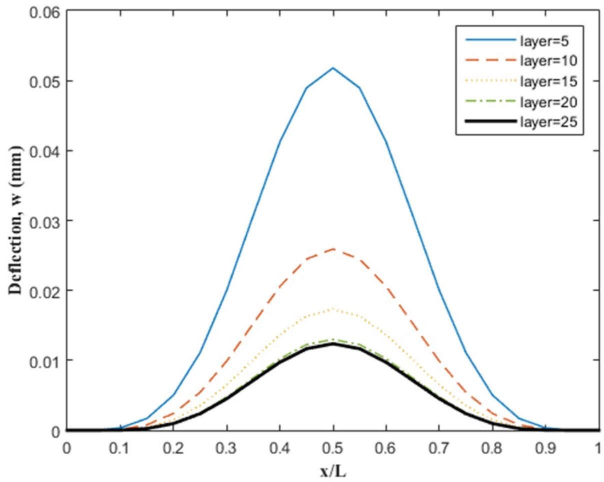

Fig. 3. Effect of the number of layers on the static deflection of the structure at the beginning of the loading stage.

6.2. Validation of Results

First, the bending of a simple curved beam without SMA is validated. For this purpose, a curved beam with an elastic modulus of 130GPa, Poisson's ratio of 0.34, density of 8960kg/m^3, angle of 60°,and length-to-radius ratio of 20 is considered, and the dimensionless static deflection $(W = w/h)$ in terms of the dimensionless load $P = \dfrac{ql^3}{EI}$ is shown in Fig. 4. As shown, the static deflection of this project is in good validation with the article of Anirudh et al. [35].

For another validation of this work, the results of this research are compared with the three-point bending test for a straight SMA beam with simple two-end boundary conditions conducted by Eshghinejad and Elahinia [36]. The properties of SMA in this part are shown in Table 3.

For comparison, a beam with a length of 49.92mm, width of 2.9mm, and thickness of 0.95mm is considered. The deflection at the beam's center is shown in Fig. 5 in terms of the transverse force. As can be seen in the figure, in both loading and unloading parts, the results of this research have an acceptable agreement with the results of Eshghi Nejad and Elahini [36]. The reason for the small difference in the elastic part between the results of this report and Ref. [36] is the different models and solution methods. In this paper, DQM is used, while in the article by Eshghi Nejad and Elahini [36], the three-point bending test method is used.

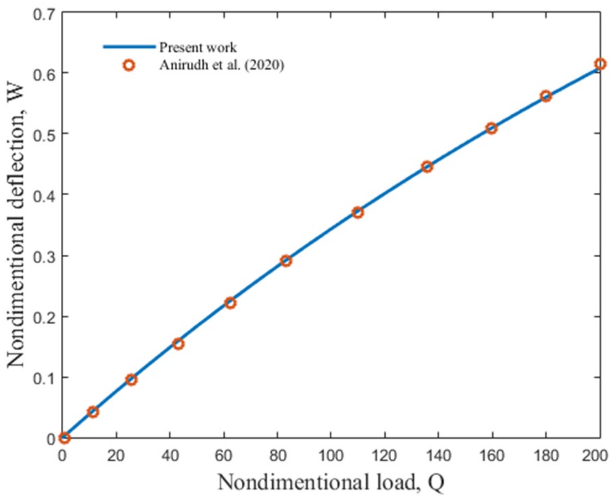

Fig. 4. Comparison of the present results with the results of Anirodeh et al. for bending analysis of the curved beam.

Table 3
Properties of nickel-titanium memory alloy [36].

Properties	Unit
A_s	0°C
A_f	2°C
M_s	−10°C
M_f	−20°C
$\upsilon^A = \upsilon^M$	0.3
E_A	73.2GPa
E_M	30GPa
C_M	5MPa/°C
C_A	10MPa/°C
σ^{cr}	0MPa
σ^{cr}	100MPa

6.3. Quasi-Static Analysis of the SMA Curved Beam

Fig. 6 shows the changes of stress against strain for a different curvature radius of the curved beam for the middle point of the beam and the upper layer. As can be inferred from the figure, with the increase in the curved beam's curvature radius, the area of hysteresis loop increases, which indicates a decrease in the strength of the structure. The effect of the curvature radius of the curved beam for the middle point of the beam and the upper layer on the deflection is shown in Figs. 7 and 8 for the beginning of the loading stage and the end of the loading stage, respectively. As it can be seen, with the increase of the curvature radius of the curved beam, the deflection increases because with the increase of the curvature radius, the stiffness of the structure decreases.

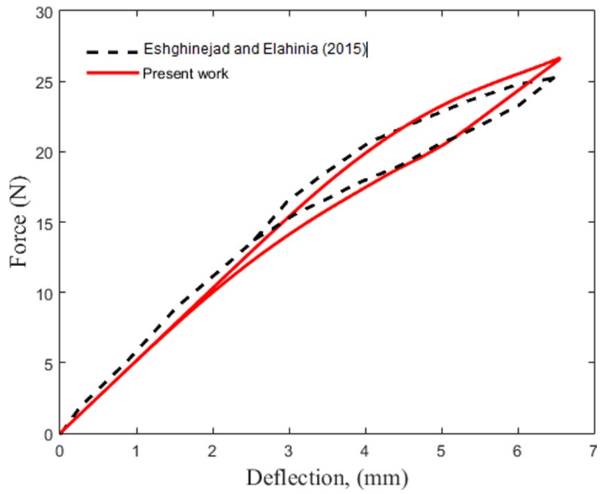

Fig. 5. Comparison of the results of this research with the three-point bending test of a straight SMA beam.

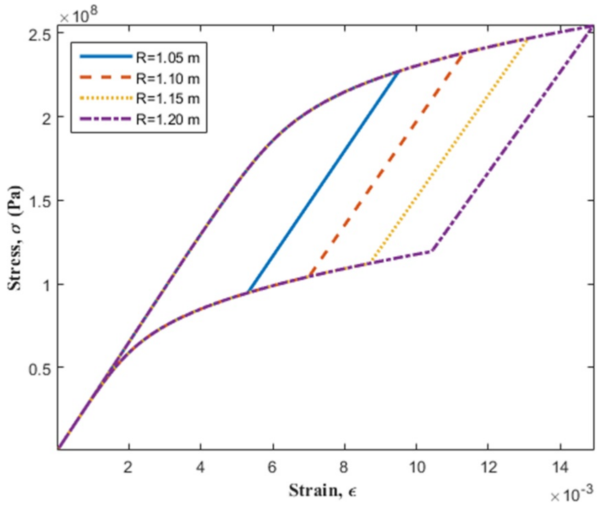

Fig. 6. Effect of curvature radius on the stress-strain diagram of the SMA curved beam.

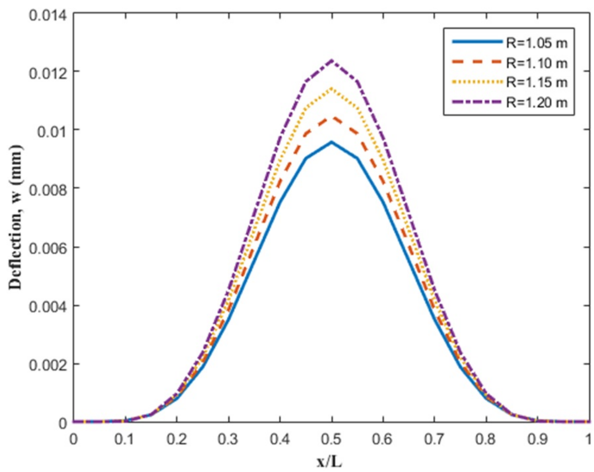

Fig. 7. Effect of curvature radius on the static deflection of the structure at the beginning of the loading stage.

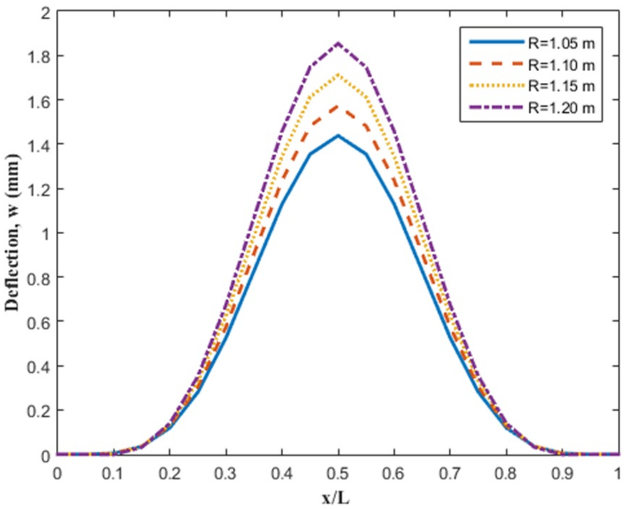

Fig. 8. Effect of curvature radius on the static deflection of the structure at the end of the loading stage.

The distribution of martensite volume fraction for the loading and unloading stages at different points of the clamped-clamped beam is drawn in Fig. 9 for the top layer. On the longitudinal axis, up to number 300 is related to loading and the range from 300 to 600 is related to unloading and q_0 is considered to be equal to 0.01N/m. It can be seen that on the left side of the beam ($x = 0$), the martensite volume fraction has the highest value and as it approaches the center of the beam, this value decreases.

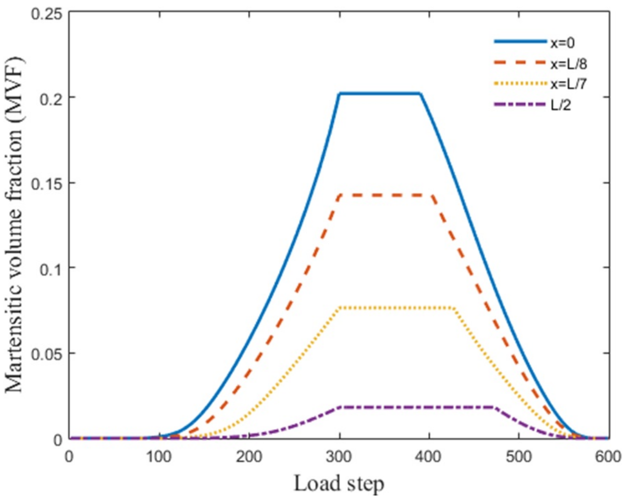

Fig. 9. Distribution of martensite volume fraction for different stages of loading and unloading.

Fig. 10 shows the changes of stress against strain for various boundary supports for the middle point of the beam and the upper layer. As can be inferred from the figure, the clamped-clamped curved beam has the lowest area of hysteresis loop. Figs. 11 and 12 show the effect of the boundary supports on the deflection for the middle point of the beam and the upper layer for two stages a) the beginning of the loading stage and b) the end of the loading stage, respectively. As it can be seen, the clamped-clamped curved beam has lower deflection with respect to the simply-simply and clamped-simply curved beam due to more bending rigidity. In other words, the maximum deflection for the clamped- clamped curved beam is 1.857mm while it is 2.224mm for the simply-simply curved beam, which shows a reduction in deflection by approximately 20%.vspace2mm

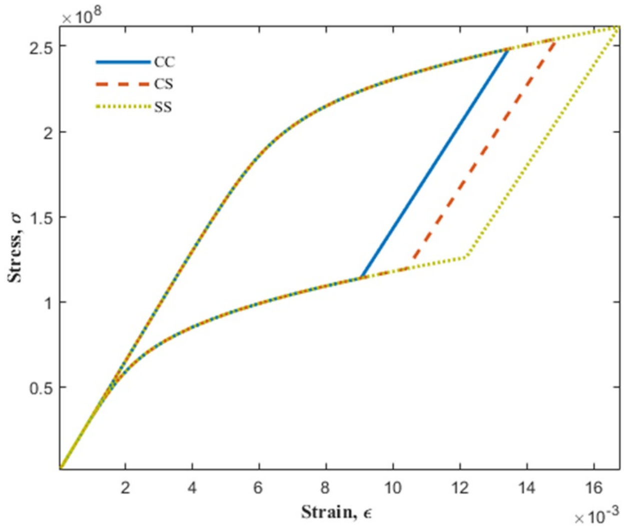

Fig. 10. Effect of the boundary supports on the stress-strain diagram of the SMA curved beam.

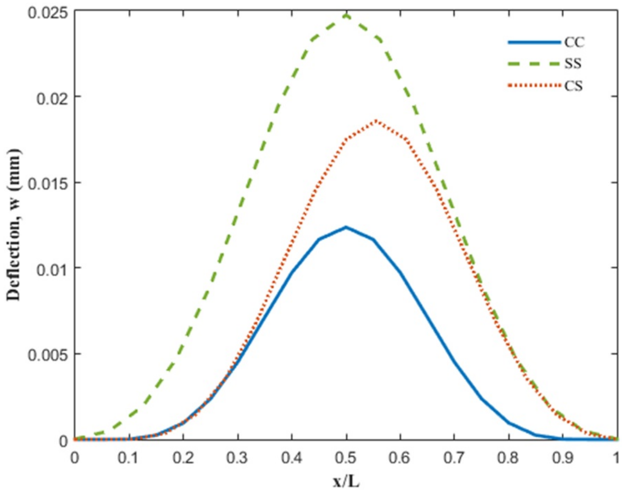

Fig. 11. Effect of the boundary supports on the static deflection of the structure at the beginning of the loading stage.

7. Conclusions

The main objective of this paper was to obtain the martensite volume fraction, stress, and strain for all points of the beam. To validate this paper, results of static bending of a straight beam made of SMA using DQM were confirmed with other researchers' works. Numerical results show that with the increase in the curvature radius of the curved beam, the area of the hysteresis loop is increased, indicating a decrease in the strength of the structure and, consequently, an increase in the static deflection. In addition, some new outcomes were studied for various boundary conditions. In the case of clamped-clamped curved beam, it was concluded that at the beam's ends, the martensite volume fraction had the highest value and that as it approached the center of the beam, this value decreased.

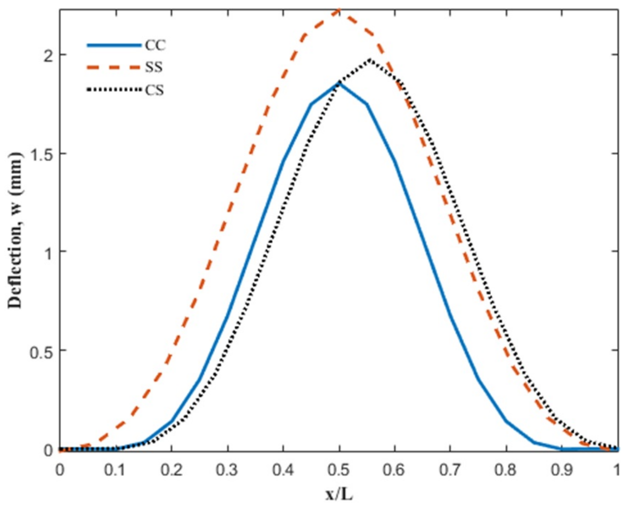

Fig. 12. Effect of the boundary supports on the static deflection of the structure at the end of the loading stage.

In this research, a quasi-static analysis of curved beam made of SMA was investigated. The 3D Hernandez-Lagoudas model was used to express the nonlinear behavior of the SMA curved beam. For the mathematical modeling of the SMA curved beam, the Timoshenko beam theory was applied considering the nonlinear strains. Then, the governing equations were extracted using Hamilton's principle. The kinematic equations of SMAs were coupled with the governing equations of the beam, which made the analysis more complex. To solve the nonlinear governing equations, DQM in conjunction with the Newton–Raphson method was utilized.

The purpose of this paper was to calculate the martensite volume fraction, stress, and strain for all points and layers of the curved beam. To validate the presented research and solution method, the static bending of a SMA beam was presented and the obtained outcomes were validated with the other papers. From the results of this research, it can be found that with the increase in the curvature radius of the curved beam, the area of hysteresis loop increased, indicating a decrease in the strength of the structure. It can also be seen that with the increase in the curvature radius of the beam, the deflection increased. In addition, for the clamped boundary conditions on the left side of the beam, the martensite volume fraction had the highest value and as it approached the center of the beam, this value decreased.

References

[1] Y. Wu, Y. Wu, Y. Wang, W. Zhong, Study on the response to low-velocity impact of a composite plate improved by shape memory, Acta Mech. Solida Sinica, 20 (2007) 357-362.

[2] S.M.R. Khalili, A. Shokuhfar, F. Ashenai Ghasemi, Effect of smart stiffening procedure on low-velocity impact response of smart structures, J. Mat. Proces. Technol., 190 (2007) 142–152.

[3] S.M.R. Khalili, A. Shokuhfar, K. Malekzadeh, F. Ashenai Ghasemi, Low-velocity impact response of active thin-walled hybrid composite structures embedded with SMA wires, Thin-Walled Struct. , 45 (2007) 799–808.

[4] A. Shokuhfar, S.M.R. Khalili, F. Ashenai Ghasemi, K. Malekzadeh, S. Raissi, Analysis and optimization of smart hybrid composite plates subjected to low-velocity impact using the response surface methodology (RSM), Thin-Walled Struct. , 46 (2008) 1204– 1212.

[5] E.H. Kim, I. Lee, J.H. Roh, J.S. Bae, I.H. Choi, K.N. Koo, Effects of SMAs on low velocity impact characteristics of composite plate, Compos. Struct., 93 (2011) 2903-2909.

[6] S.M.R Khalili, M. Botshekanan Dehkordia, M.Shariyat, Modeling and transient dynamic analysis of pseudoelastic SMA hybrid composite beam, Appl. Math. Comput., 219 (2013) 9762-9782.

[7] B. Liu, G. Dui, S. Yanga, On the transformation behavior of functionally graded SMA composites subjected to thermal loading, Eur. J. Mech. A. Solids, 40 (2013) 139-147.

[8] S.M.R Khalili, M. Botshekanan Dehkordia, E. Carrera, M. Shariyat, Non-linear dynamic analysis of a sandwich beam with pseudoelastic SMA hybrid composite faces based on higher order finite element theory, Compos. Struct., 96 (2013) 243-255.

[9] H. Asadi, Y. Kiani, M. Shakeri, M.R. Eslami, Exact solution for nonlinear thermal stability of hybrid laminated composite Timoshenko beams reinforced with SMA fibers, Compos. Struct., 108 (2014) 811-822.

[10] H. Asadi, Y. Kiani, M. Shakeri, M.R. Eslami, Exact solution for nonlinear thermal stability of geometrically imperfect hybrid laminated composite Timoshenko beams embedded with SMA fibers, J. Eng. Mech., 141 (2015) 04014144.

[11] M. Botshekanan Dehkordi, S.M.R. Khalili, E. Carrera, Non-linear transient dynamic analysis of sandwich plate with composite face-sheets embedded with SMA wires and flexible core-based on the mixed LW (layer-wise)/ESL (equivalent single layer) models, Compos. Part B: Eng., 87 (2016) 59-74.

[12] D. Hu, L. Zhang, R. Wang, X. Zhang, Investigation on low velocity impact resistance of SMA composite material, Composite Structures, SPIE Smart Struct. Mat., 23 (2016) 451-466.

[13] D.M. Junior, M.V. Donadon, S.G.P. Castroa, Aeroelastic behavior of stiffened composite laminated panel with embedded SMA wire using the hierarchical Rayleigh–Ritz method, Compos. Struct., 181 (2017) 26-45.

[14] Y. Bayat, H. Ekhteraei, Exact solution of thermal buckling and post buckling of composite and SMA hybrid composite beam by layerwise theory, Aerosp. Sci. Technol., 67 (2017) 484-494.

[15] Y. Bayat, H. Ekhteraei, Exact solution of thermal buckling and post buckling of composite and SMA hybrid composite beam by layerwise theory, Aerosp. Sci. Technol., 67 (2017) 484-494.

[16] M.Z. Kabir, B.T. Tehrani, Closed-form solution for thermal, mechanical, and thermo-mechanical buckling and post-buckling of SMA, Compos. Struct., 168 (2017) 535-548.

[17] P. Fahimi, A. H. Eskandari, M. Baghani, A. Taheri. A semi-analytical solution for bending response of SMA composite beams considering SMA asymmetric behavior, Compos. Part B: Eng., 163 (2019) 622–633.

[18] A. Ali, A. L. Conte, C. A. Biffi, A. Tuissit, Cohesive Surface Model for Delamination and Dynamic behavior of Hybrid Composite with SMA-GFRP Interfacei, Int. J. Lightweight Mat. Manuf., 2 (2019) 146-155.

[19] M. Karimiasl, F. Ebrahimi, B. Akgözb, Buckling and post-buckling responses of smart doubly curved composite shallow shells embedded in SMA fiber under hygro-thermal loading, Compos. Struct., 223 (2019) 479–492.

[20] M. H. Enferadi, M. R. Ghasemi, N. Shabakhty, Wave-induced vibration control of offshore jacket platforms through SMA dampers, Appl. Ocean Res., 90 (2019) 479–492,

[21] M. Nejati, A. G. Ghalebahman, A. Soltanimaleki, R. Dimitri, Thermal vibration analysis of SMA hybrid composite double curved sandwich panels, Compos. Struct., 224 (2019) 622–633.

[22] Y. Suzuki, Y. Kagawa, Dynamic tracking control of an SMA wire actuator based on model matching, Sens. Actuators, A, 292 (2019) 129–136.

[23] Y. Bayat, H. E.Toussi, A nonlinear study on structural damping of SMA hybrid composite beam, Thin-Walled Struct., 134 (2019) 18–28.

[24] E. Shafeia, R. Kianoush, Transient analysis of hybrid SMA-FRP reinforced concrete beams under sequential impacts, Eng. Struct., 208 (2020) 109915.

[25] A. Fallah, M. Botshekanan Dehkordi, S.H. Nourbakhsh, Nonlinear dynamic analysis of microbeam containing graded shape memory microwires, Compos. Struct., 257 (2021) 113085.

[26] M.R. Aghababaiyan, M. Botshekanan Dehkordi, A. Fallah, Investigation of nonlinear dynamic behavior of micro-beam reinforced with CNT containing SMA micro-wires considering size effect, J. Braz. Soc. Mech. Sci. Eng. 43 (2021) 481-499.

[27] A. Fallah, M. Botshekanan Dehkordi, A new nonlinear finite element model for transient dynamic response of a micro composite plate embedded with micro SMA wires considering the size effects, Mech. Advan. Mat. Struct., (2021), In press, https://doi.org/10.1080/15376494.2021.1983900.

[28] S. Kamarian, J.I. Song, A comparative study on the effect of SMAs and CNTs on the vibration of composite plates exposed to thermal environments, Case Stud. Therm. Eng., 36 (2022) 102121.

[29] M. Shariyat, M. Mirmohammadi, Comparing the Modified Strain Gradient, Modified Couple Stress, and Classical Results for Vibration Dissipation of SMA-Wire-Reinforced Microplates with Nonidentical Size-Effect Coefficients, Iran. J. Sci. Technol., Transactions of Mechanical Engineering, (2022), In press, https://doi.org/10.1007/s40997-022-00531-y.

[30] D.C. Lagoudas, D. Hartl, Y. Chemisky, L. Machado, P. Popov, Constitutive model for the numerical analysis of phase transformation in polycrystalline SMAs. Int. J. Plasticity, 32 (2012) 155-183.

[31] J.N. Reddy, An Introduction to Nonlinear Finite Element Analysis. Oxford: Oxford University Press (2005).

[32] A. Cheraghbak, M. Botshekanan Dehkordi, H. Golestanian, Vibration analysis of sandwich beam with nanocomposite facesheets considering structural damping effects, Steel Compos. Struct., 32 (2019) 795-806.

[33] D.C. Lagoudas, SMAs. Modeling and Engineering Applications, springer; (2007).

[34] K. Jacobus, H. Sehitoglu, M. Balzer, Effect of stress state on the stress-induced martensitic transformation in polycrystalline Ni–Ti alloy, Metallurgical Mat. Transact. A, 27 (1996) 3066–3073.

[35] B. Anirudh, T. Ben Zine, O. Polit, M Ganapathi, G. Prateek, Nonlinear bending of porous curved beams reinforced by functionally graded nanocomposite graphene platelets applying an efficient shear flexible finite element approach, Int. J. Non-Linear Mech., 119 (2020) 103346.

[36] A. Eshghinejad, M. Elahinia, Exact Solution for Bending of SMA Beams, Mech. Advan. Mat. Struct., 22 (2015) 829-838.